On the Effect of Sheath, Collision, and Absorptive Surface on the Performance of a Linear Antenna in a Compressible Plasma

SING-HSIUNG LIN, MEMBER, IEEE, AND KENNETH K. MEI, MEMBER, IEEE

Abstract—**The boundary value problem posed by a linear antenna with sheath or absorptive surface in a compressible lossy plasma is formulated in terms of coupled integral equations. The integral equations are solved with the aid of a digital computer. The results presented here include the effects of sheath, collision, and absorptive surfaces on the current distribution, resonance, and antiresonances of the antenna. The analysis is most conveniently applied in studying an electrically short antenna which is of the order of several electroacoustic wavelengths long.**

Introduction

IN A PREVIOUS paper [1], the authors have presented an analysis of a sheathless finite cylindrical antenna in an isotropic homogeneous compressible lossless plasma. In this paper the effect of sheath on the performance of an antenna in a lossy plasma is investigated. Sheath effect has been reported by Carlin and Mittra [2] for a finite biconical antenna with a spherical sheath, by Lytle and Schultz [3] for a prolate spheroidal antenna, by Wait and Spies [4] for a spherical antenna, and by Galejs [5] for a finite cylindrical antenna in an infinitely long cylindrical sheath.

A common feature in the previous investigations on sheath effect is that the antenna surface or the sheath surface is assumed to be rigid. In this paper, we shall include both the collision effect and absorptive surface in the analyses.

This absorptive surface is represented by the boundary condition

$$\hat{n} \cdot (\bar{v}/v_0) = \alpha(n_1/n_0) \qquad (1)$$

from which the special case of a rigid surface may be obtained for $\alpha = 0$.

The effects of loss, sheath, and absorptive surface on the antenna performance are presented.

Manuscript received January 16, 1970; revised April 13, 1970. This research was sponsored by the National Science Foundation under Grant GK-2553 and by the Joint Services Electronics Program under Contract AFOSR-68-1488.

S. H. Lin was with the Electronics Research Laboratory, University of California, Berkeley, Calif. He is now with Bell Telephone Laboratories, Inc., Holmdel, N. J. 07733.

K. K. Mei is with the Department of Electrical Engineering and Computer Sciences, Electronics Research Laboratory, University of California, Berkeley, Calif. 94720.

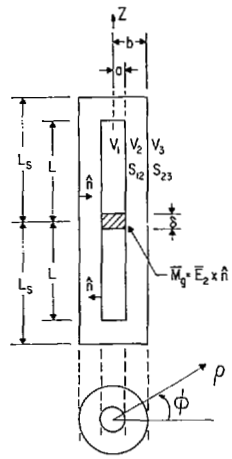

Fig. 1. Configuration of dipole antenna with sheath in plasma.

The Antenna Configuration

The configuration of the finite length cylindrical antenna in the plasma with an insulating sheath is shown in Fig. 1. The antenna will be considered as a scatterer which is illuminated by a finite source $\boldsymbol{M}_g$. If $\boldsymbol{M}_g = -\hat{\phi} \exp(j\omega t) V_g/\delta$ is a band of magnetic current of width δ and is wrapped around the cylindrical scatterer, it is equivalent to an antenna excited by a uniform axial electric field $E_z = -V_g/\delta$ in a gap of width δ, where V_g is the applied voltage.

The region V_1 is the antenna body made of perfect conductor, the region V_2 is the insulation sheath assumed to be free space, and the region V_3 is the homogeneous isotropic compressible lossy plasma. In view of the assumed rotational symmetry about the z axis, the magnetic field has a ϕ component only.

Basic Equations for Fields and Sources in the Plasma

We shall use the linearized hydrodynamic and Maxwell's equations for a one fluid plasma model. Since the equivalent source principle will be applied to derive the integral equations, the basic equations should include not only the realistic sources but also the mathematically equivalent sources. These sources are assumed to be bounded within a finite space and are of exp ($j\omega t$) time dependence.

The fields and sources in the homogeneous isotropic compressible lossy plasma may then be described by the following linearized equations:

$$\nabla \times \boldsymbol{E} + j\omega\mu_0 \boldsymbol{H} = -\bar{M} \tag{2}$$

$$\nabla \times \boldsymbol{H} - j\omega\epsilon_0 \boldsymbol{E} + en_0\bar{v} = \bar{J} \tag{3}$$

$$\mu_0 \nabla \cdot \boldsymbol{H} = \rho_m \tag{4}$$

$$\epsilon_0 \nabla \cdot \boldsymbol{E} + en_1 = \rho_e \tag{5}$$

$$n_0 \nabla \cdot \bar{v} + j\omega n_1 = Q \tag{6}$$

$$j\omega n_0 m\bar{v} + n_0 e\boldsymbol{E} + mv_0^2 \nabla n_1 + n_0 mv\boldsymbol{v} = \boldsymbol{F} \tag{7}$$

$$\nabla \cdot \bar{J} + j\omega\rho_e = eQ \tag{8}$$

$$\nabla \cdot \bar{M} + j\omega\rho_m = 0 \tag{9}$$

where ν is the effective collision frequency, ρ_e is the electric charge source, and ρ_m is the magnetic charge source. The rest of the symbols are standard and are defined in [1].

Substituting (2) and the curl of (7) into the curl of (3), we get the vector Helmholtz equation for $\boldsymbol{H}$,

$$(\nabla^2 + k_e^2)\boldsymbol{H} = -\nabla \times \left[J + \frac{je\boldsymbol{F}}{\omega m(1 - j(\nu/\omega))} \right] + j\omega\epsilon_0\epsilon_e \boldsymbol{M} - \frac{1}{j\omega\mu_0} \nabla(\nabla \cdot \bar{M}). \tag{10}$$

Substituting (5), (6), and the divergence of (7) into the divergence of (3) we get the Helmholtz equation for n_1,

$$(\nabla^2 + k_p^2) n_1 = \nabla \cdot \left[\frac{\bar{F}}{mv_0^2} + \frac{\bar{J}}{j\omega e D^2} \right] - \frac{j\omega}{v_0^2} \epsilon_p Q \tag{11}$$

where

$$\omega_p = \left[\frac{n_0 e^2}{\epsilon_0 m} \right]^{1/2} = \text{angular plasma frequency}$$

$$\epsilon_e = 1 - \frac{\omega_p^2}{\omega^2} \left(\frac{1}{1 - j(\nu/\omega)} \right)$$

$$k_e^2 = \omega^2 \mu_0 \epsilon_0 \epsilon_e$$

$$D = \frac{v_0}{\omega_p}$$

$$\lambda_D = \frac{1}{\sqrt{3}} \frac{v_0}{\omega_p} = \text{Debye length}$$

$$\epsilon_p = 1 - j\frac{\nu}{\omega} - \frac{\omega_p^2}{\omega^2}$$

$$k_p^2 = \frac{\omega^2}{v_0^2} \epsilon_p.$$

Fields in the Plasma Region V_3

The fields in the plasma region V_3 may be obtained from (10) and (11) and simple integral identities which give

$$\bar{H}(\bar{r}) = \int_{V_\infty} \left\{ \left[\bar{J}(\bar{r}') + \frac{je\bar{F}(\bar{r}')}{\omega m(1 - j(\nu/\omega))} \right] \times \nabla' G_e(\bar{r}/\bar{r}') + \left[j\omega\epsilon_0\epsilon_e \bar{M}(\bar{r}') - \frac{1}{j\omega\mu_0} \nabla' \nabla' \cdot \bar{M}(\bar{r}') \right] G_e(\bar{r}/\bar{r}') \right\} dV' \tag{12}$$

$$n_1(\bar{r}) = \int_{V_\infty} \left\{ \left[\frac{\bar{J}(\bar{r}')}{j\omega e D^2} + \frac{\bar{F}(\bar{r}')}{mv_0^2} \right] \cdot \nabla' G_p(\bar{r}/\bar{r}') + \frac{j\omega}{v_0^2} \epsilon_p Q(\bar{r}') G_p(\bar{r}/\bar{r}') \right\} dV' \tag{13}$$

where

$$G_p(\bar{r}/\bar{r}') = \frac{\exp(-jk_p |\bar{r} - \bar{r}'|)}{4\pi |\bar{r} - \bar{r}'|}. \tag{14}$$

The fields in V_3 may be reproduced by a set of equivalent sources on the surface S_{23} which are related to the fields on S_{23} by the following relations:

$$\begin{aligned} \bar{M}_3(\bar{r}) &= \bar{E}_3(\bar{r}) \times [-\hat{n}(\bar{r})] \\ \bar{J}_3(\bar{r}) &= -\hat{n}(\bar{r}) \times \bar{H}_3(\bar{r}) \\ \bar{F}_3(\bar{r}) &= mv_0^2 n_1(\bar{r}) [-\hat{n}(\bar{r})] \\ Q(\bar{r}) &= n_0 [-\hat{n}(\bar{r})] \cdot \bar{v}(\bar{r}) \\ \rho_e(\bar{r}) &= \epsilon_0 \bar{E}_3(\bar{r}) \cdot [-\hat{n}(\bar{r})] \\ \rho_m(\bar{r}) &= \mu_0 \bar{H}_3(\bar{r}) \cdot [-\hat{n}(\bar{r})]. \end{aligned} \tag{15}$$

The subscript 3 in (15) indicates its relevance to V_3. The normal $\hat{n}$ is pointed away from V_3. Owing to the symmetry of the problem, $\boldsymbol{H}$ contains the ϕ component only. Therefore,

$$\nabla \cdot \boldsymbol{M} = -j\omega\rho_m = j\omega\mu_0 [-\hat{n}] \cdot \boldsymbol{H} = 0. \tag{16}$$

Replacing the sources in (12) by the equivalent sources of (15) and letting the observation point $\boldsymbol{r}$ to approach the surface S_{23}, we find the tangential component of $\bar{H}$ to satisfy the integral equation

$$-\tfrac{1}{2}\hat{n} \times \bar{H}_3(\bar{r}) = P \int_{S_{23}} \hat{n} \times \left\{ \left[-\hat{n}' \times \bar{H}_3(\bar{r}') + \frac{jev_0^2 n_1(\bar{r}')(-\hat{n}')}{\omega(1 - j(\nu/\omega))} \right] \times \nabla' G_e(\bar{r}/\bar{r}') + j\omega\epsilon_0\epsilon_e [\bar{E}_3(\bar{r}') \times (-\hat{n}')] G_e(\bar{r}/\bar{r}') \right\} ds'. \tag{17}$$

A similar limiting process gives $n_1(r)$ as

$$\tfrac{1}{2}n_1(r) = P\int_{S_{23}} \left\{\left[\frac{-\hat{n}'\times\bar{H}_3(\bar{r}')}{j\omega\epsilon D^2} + n_1(\bar{r}')(-\hat{n}')\right] \cdot\nabla' G_p(\bar{r}/\bar{r}') - \frac{j\omega}{v_0^2}\epsilon_p n_0 \hat{n}'\cdot\bar{v}(\bar{r}')G_p(\bar{r}/\bar{r}')\right\} ds' \quad (18)$$

where P denotes the principal value of the integral.

Equations (17) and (18) are two of the integral equations for the three unknown functions $\hat{n}\times\bar{H}_3(\bar{r})$, $\hat{n}\times\bar{E}_3(\bar{r})$, and $n_1(\bar{r})$ on the surface S_{23}.

Fields in the Sheath Region V_2

The insulation sheath as depicted in Fig. 1 is assumed to be an homogeneous dielectric. Therefore, only electromagnetic fields exist in this region. Using the equivalent source principle the fields in V_2 may be reproduced by the surface sources which are

$$\left.\begin{aligned}\bar{M}_2(\bar{r}) &= \bar{E}_2(\bar{r})\times\hat{n}(\bar{r})\\ \bar{J}_2(\bar{r}) &= \hat{n}(\bar{r})\times\bar{H}_2(\bar{r})\end{aligned}\right\} \text{ on } S_{23}$$

$$\left.\begin{aligned}\bar{M}_1(\bar{r}) &= \bar{E}_2(\bar{r})\times\hat{n}(\bar{r})\\ \bar{J}_1(\bar{r}) &= \hat{n}(\bar{r})\times\bar{H}_2(\bar{r})\end{aligned}\right\} \text{ on } S_{12}. \quad (19)$$

The preceding equivalent sources will reproduce the fields in V_2 but null field in regions V_1 and V_3. Also, $\bar{M}_1(r)$ is a known function because on the antenna surface $\hat{n}\times\boldsymbol{E}$ vanishes except at the driving gap.

Using the same approach as in V_3 we get the integral equations for the tangential component of $\boldsymbol{H}(r)$ in V_2 to be

$$\begin{aligned}\tfrac{1}{2}\hat{n}\times\bar{H}_2(\bar{r})\,|_{S_{23}} = P\int_{S_{23}} &\hat{n}\times\{[\hat{n}'\times\bar{H}_2(\bar{r}')]\times\nabla' G_0(\bar{r}/\bar{r}) \\ &+ j\omega\epsilon_0[\bar{E}_2(\bar{r}')\times\hat{n}']G_0(\bar{r}/\bar{r}')\}\,ds' \\ &+ \int_{S_{12}} \hat{n}\times\{[\hat{n}'\times\bar{H}_2(\bar{r}')]\times\nabla' G_0(\bar{r}/\bar{r}') \\ &+ j\omega\epsilon_0[\bar{E}_2(\bar{r}')\times\hat{n}']G_0(\bar{r}/\bar{r}')\}\,ds' \quad (20)\end{aligned}$$

and

$$\begin{aligned}&\tfrac{1}{2}\hat{n}\times\boldsymbol{H}_2(\bar{r})\,|_{S_{12}} \\ &= \int_{S_{23}} \hat{n}\times\{[\hat{n}'\times\bar{H}_2(\bar{r}')]\times\nabla' G_0(\bar{r}/\bar{r}') \\ &\quad + j\omega\epsilon_0[\bar{E}_2(\bar{r}')\times\hat{n}']G_0(\bar{r}/\bar{r}')\}\,ds' \\ &\quad + P\int_{S_{12}} \hat{n}\times\{[\hat{n}'\times\bar{H}_2(\bar{r}')]\times\nabla' G_0(\bar{r}/\bar{r}') \\ &\quad + j\omega\epsilon_0[\bar{E}_2(\bar{r}')\times\hat{n}']G_0(\bar{r}/\bar{r}')\}\,ds' \quad (21)\end{aligned}$$

where we have assumed the sheath to be free space; thus

$$G_0(\bar{r}/\bar{r}') = \frac{\exp(-jk_0|\bar{r}-\bar{r}'|)}{4\pi|\bar{r}-\bar{r}'|}. \quad (22)$$

Equations (20) and (21) provide the additional two integral relations for the fields on the boundaries.

Boundary and Continuity Conditions

The boundary conditions for the antenna and its sheath are

$$\bar{E}_2(\bar{r})\times\hat{n} = \begin{cases}0, & \text{for } |z| > \delta/2 \quad \text{on } S_{12}\\ M_g, & \text{for } |z| \le \delta/2 \quad \text{on } S_{12}\end{cases} \quad (23)$$

where M_g is the equivalent driving source previously defined. The absorptive boundary condition

$$\frac{\hat{n}\cdot\bar{v}(\bar{r})}{v_0} = \alpha\frac{n_1(\bar{r})}{n_0} \quad \text{on } S_{23} \quad (24)$$

was suggested by Balmain [6], Wait [7], and Sancer [8]. α is a dimensionless parameter related to the acoustic surface impedance.

The continuity condition at the sheath are

$$\begin{aligned}\hat{n}\times\bar{H}_2(\bar{r}) &= \hat{n}\times\bar{H}_3(\bar{r}) \quad \text{on } S_{23}\\ \hat{n}\times\bar{E}_2(\bar{r}) &= \hat{n}\times\bar{E}_3(\bar{r}) \quad \text{on } S_{23}. \quad (25)\end{aligned}$$

The Integral Equations

Applying the boundary and continuity conditions to (17), (18), (20), and (21), and specializing the equations for cylindrical antennas we get the following coupled integral equations:

$$\begin{aligned}\tfrac{1}{2}H_{\phi 23}(z) = &-P\left\{\int_{S_{23}} H_{\phi 23}(z')\left.\frac{\partial G_e(\bar{r}/\bar{r}')}{\partial\rho}\right|_{\rho=b} ds'\right. \\ &- \frac{jev_0^2}{\omega(1-j(\nu/\omega))}\int_{S_{23}} n_1(z')\left.\frac{\partial G_e(\bar{r}/\bar{r}')}{\partial z}\right|_{\rho=b} \\ &\cdot\cos(\phi-\phi')\,ds' + j\omega\epsilon_0\epsilon_e \\ &\left.\cdot\int_{S_{23}} E_{z23}(z')G_e(\bar{r}/\bar{r}')\cos(\phi-\phi')\,ds'\right\} \quad (26)\end{aligned}$$

$$\begin{aligned}\tfrac{1}{2}H_{\phi 23}(z) = &-P\left\{\int_{S_{23}} -H_{\phi 23}(z')\left.\frac{\partial G_0}{\partial\rho}(\bar{r}/\bar{r}')\right|_{\rho=b} ds' + j\omega\epsilon_0\right. \\ &\cdot\int_{S_{23}} E_{\phi 23}(z')G_0(\bar{r}/\bar{r}')\Big|_{\rho=b}\cos(\phi-\phi')\,ds' \\ &+ \int_{S_{12}} H_{\phi 12}(z')\left.\frac{\partial G_0(\bar{r}/\bar{r}')}{\partial\rho}\right|_{\rho=b} ds' \\ &\left.+ j\omega\epsilon_0\frac{V_g}{\delta}\int_{S_g} G_0(r/r')\Big|_{\rho=b}\cos(\phi-\phi')\,ds'\right\} \quad (27)\end{aligned}$$

where S_g is the portion of S_{12} covered by the driving gap

$$\tfrac{1}{2}n_1(z) = P\Big\{\int_{S_{23}} n_1(z')\left[\frac{\partial G_p(\bar{r}/\bar{r}')}{\partial \rho'}\Big|_{\rho=b} - \alpha\frac{j\omega}{v_0}\epsilon_p G_p(\bar{r}/\bar{r}')\right]ds' + \frac{1}{j\omega e D^2} \cdot \int_{S_{23}} H_{\phi 23}(z')\,\frac{\partial G_p(\bar{r}/\bar{r}')}{\partial z'}\Big|_{\rho=b} ds'\Big\} \tag{28}$$

$$\tfrac{1}{2}H_{\phi 12}(z) = -P\Big\{\int_{S_{23}} - H_{\phi 23}(z')\,\frac{\partial G_0(\bar{r}/\bar{r}')}{\partial \rho}\Big|_{\rho=a} ds' + j\omega\epsilon_0 \cdot \int_{S_{23}} E_{z23}(z')G_0(\bar{r}/\bar{r}')\Big|_{\rho=a}\cos(\phi-\phi')\,ds' + \int_{S_{12}} H_{\phi 12}(z')\,\frac{\partial G_0(\bar{r}/\bar{r}')}{\partial \rho}\Big|_{\rho=a} ds' + j\omega\epsilon_0\frac{V_g}{\delta} \cdot \int_{S_g} G_0(\bar{r}/\bar{r}')\Big|_{\rho=a}\cos(\phi-\phi')\,ds'\Big\}. \tag{29}$$

The mechanical force on the sheath surface is given by

$$\bar{F}(\bar{r}) = mv_0^2 n_1(\bar{r})[-\hat{n}] \quad \text{on } S_{23}. \tag{30}$$

Accuracy of the Numerical Solutions

The preceding derived integral equations may be solved numerically by the method of collocation using finite zoning functions and quadratic interpolations. This method is described briefly in [1]. Readers interested in the details of this method are referred to [9]–[12]. For numerical integration of the singular functions, the method of auxiliary integral described by Lin and Mei [1] is used.

The accuracy of the numerical solutions of integral equations depends on many factors such as the stability of the integral equation, the interpolation, the source model, and the singular integration of the kernel. We choose to demonstrate the soundness of our formulation by calculating a monopole over an infinite ground plane which has been carefully measured by Hartig, see [13]. Fig. 2 illustrates the configuration of the monopole, and Fig. 3 shows the comparison of the numerical results of our formulation and the measured input current of Hartig. Fig. 4 illustrates the convergent trend of the numerical results. In view of the ambiguity of the driving point configuration of many numerical investigations on linear antennas, the good agreement between the experimental and our numerical results indicates that the formulation of this paper, in particular the source model, is a sound one. The numerical accuracy of computations on plasmas is also checked by a convergence plot similar to that of Fig. 4. We have found that the number of subdivisions $N = 63$ (including the surface of the antenna and the sheath) is sufficient to calculate the longest antenna of this paper.

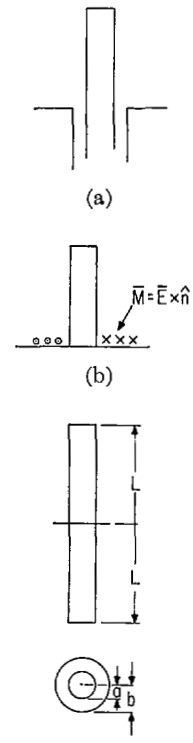

Fig. 2. (a) Monopole over ground plane, base driven from coaxial line. (b) Equivalent monopole over ground plane, driven by magnetic current. (c) Equivalent dipole in free space, driven by magnetic current.

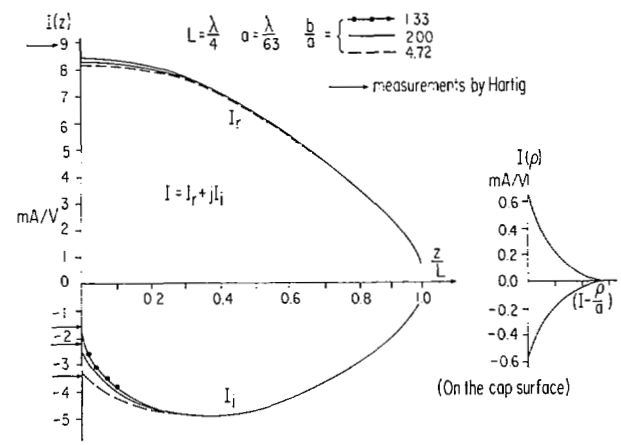

Fig. 3. Current distribution on surface of monopole antenna base driven from coaxial line.

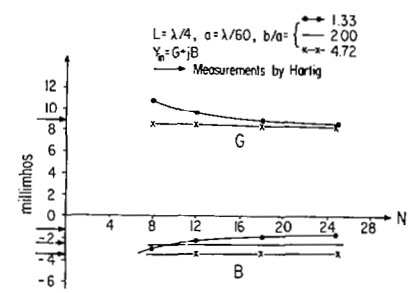

Fig. 4. Convergence of numerical solutions by method of collocation.

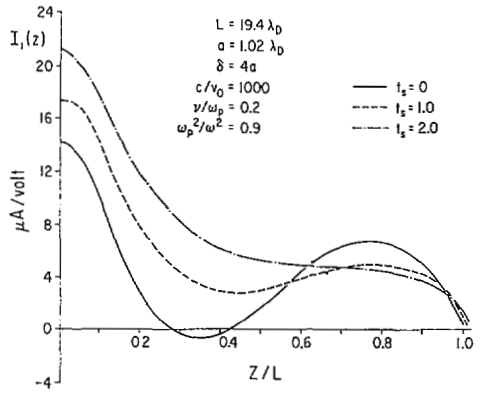

Fig. 5. Effect of sheath thickness on imaginary part of electric current distribution.

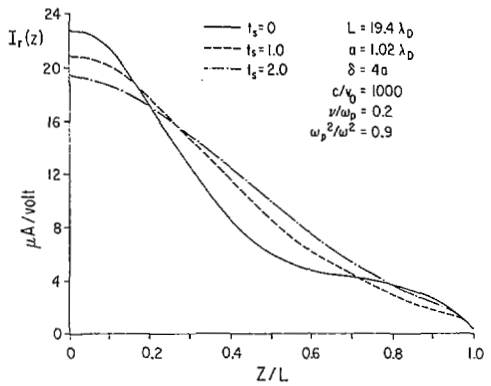

Fig. 6. Effect of sheath thickness on real part of electric current distribution.

The Effects of the Sheath on Surface Fields

We define the normalized sheath thickness as

$$t_s = (b - a)/a \tag{31}$$

where a is the radius of the antenna and b is the radius of the sheath. Figs. 5 and 6 show that the effect of increasing t_s is to decrease the wave number and amplitude of the sinusoidal component. Similar effects on the current were found by Galejs for an infinite sheath. Figs. 7 and 8 show that the sheath effect on the electron density n_1 on S_{23} is to reduce its amplitude and wavenumber as t_s increases.

Sheath Effect on the Driving Point Characteristics

Since the vacuum sheath around an antenna has an isolation effect which reduces the plasma influence on the antenna performance, it is intuitively anticipated that it reduces the radiation resistance of a short dipole. Figs. 9 and 10 give quantitative evidence of the sheath effect on the input impedance of a dipole antenna. Similar effect has been reported by other authors [4], [5], [14], and [15] for various configurations of antenna and sheath.

The isolation effect of the sheath also increases the maximum allowable driving voltage as shown in Fig. 10. The driving voltage is limited by V_{max} to insure the

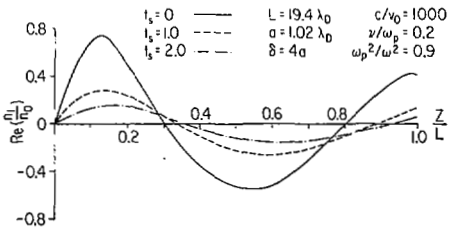

Fig. 7. Effect of sheath thickness on real part of plasma density distribution on S_{23}.

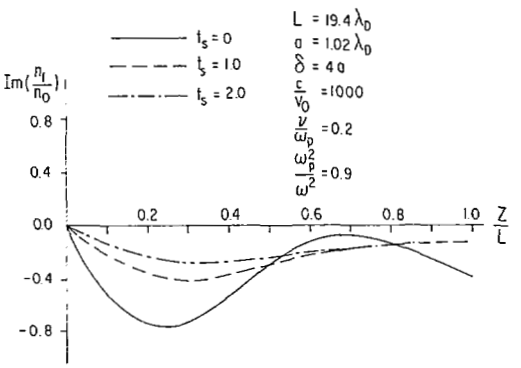

Fig. 8. Effect of sheath thickness on imaginary part of plasma density distribution on S_{23}.

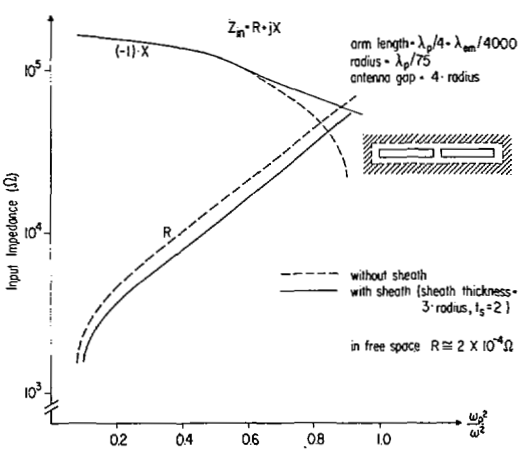

Fig. 9. Input impedance of dipole antenna in warm plasma for $\nu/\omega_p = 0$.

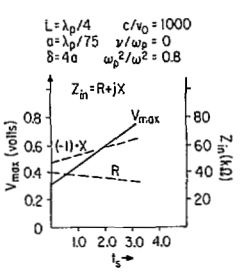

Fig. 10. Input impedance and V_{max} of sheathed antenna in lossless plasma versus sheath thickness.

linearity of the plasma [1] so that the result of this analysis may be meaningful. Indeed, experimental investigations reported by Jackson and Kane [16] and Baker and Despain [17] all indicate that the RF voltage of the antenna must be kept in the order of 1 volt or less in order to obtain meaningful experimental results.

Collision Effect and the Resonance Probes

In the plasma diagnostics using resonance probe, it is well known that a resonance on the RF current occurs at a frequency f_r below the plasma frequency f_p [18], [19]. In addition there is a less pronounced antiresonance at $f_a < f_p$, where the RF current exhibits a minimum. Many investigators have suggested using the resonance or antiresonance phenomenon as a clue to plasma diagnostics. In this investigation we have calculated the antenna admittances at the frequencies below the plasma frequency and have found strong influence on the resonance or antiresonance phenomenon due to collision.

In Fig. 11 the input admittance is shown for a cylindrical antenna of halflength $L = 3.84\lambda_D$ as a function of ω_p^2/ω^2. This halflength is chosen because $L \cong \lambda_s/4$ at $\omega_p^2/\omega^2 = 1$, where λ_s is the surface wavelength [1]. The maximum of the input conductance at $\omega_p^2/\omega^2 \leq 1$ is due to the radiation of an electroacoustic wave. When the collision frequency is zero ($\nu/\omega_p = 0$), the admittance has antiresonance at $\omega_p^2/\omega^2 = 1$. This to be expected since the relative dielectric constant $\epsilon_r = 1 - \omega_p^2/\omega^2$ approaches zero. The numerical solutions fail to converge for $\nu = 0$, $\alpha = 0$, and $\omega < \omega_p$ indicating that the solution may not be unique because the purely reactive plasma and surface wave may maintain a self-sustaining oscillation. However, the exact reason for the failure of the numerical solution under this condition is still unknown.

When the medium is lossy ($\nu/\omega_p = 0.2$), the antiresonance at $\omega_p^2/\omega^2 = 1$ is damped out, and the input admittance becomes a smooth function of ω_p^2/ω^2. For such a short antenna, the absence of any resonance or antiresonance for $\omega_p^2/\omega^2 > 1$ is also observed by Harp and Crawford [18] whose theoretical model is based on kinetic theory, while our model is based on hydrodynamic theory.

For a longer antenna ($L = 11.52\lambda_D$), Fig. 12 shows that the input conductance exhibits a maximum at $\omega_p^2/\omega^2 = 1.3$ but the input susceptance does not cross zero. The input admittance of the same antenna at reduced collision frequency is shown in Fig. 13. The strong antiresonance in this case is a convincing evidence of the importance of loss in plasma diagnostics.

For an even longer antenna ($L = 19.4\lambda_D$), Fig. 14 shows that the input admittance clearly exhibits an antiresonance at $\omega_p^2/\omega^2 \cong 1.1$ and a resonance at $\omega_p^2 \cong 1.7$. Investigators of long antennas [20], [21] have shown that the input susceptance of an antenna in plasma changes from capacitive to inductive when ω_p^2/ω^2 passes through 1.0 from below. But the aforementioned calculations on short antennas have found the antiresonance easily damped in lossy plasma. This phenomenon can best be explained

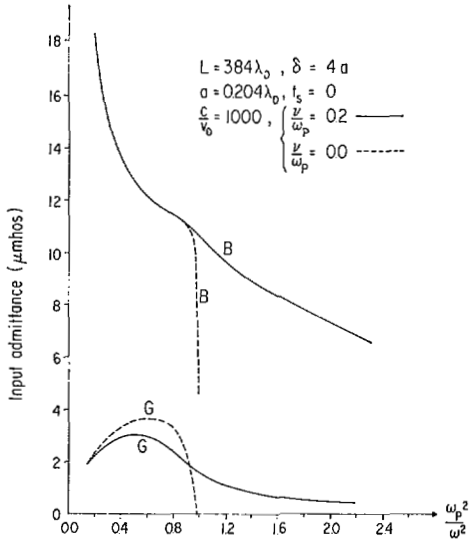

Fig. 11. Effect of loss to input admittance of dipole in warm plasma ($L = 3.84\lambda_D$).

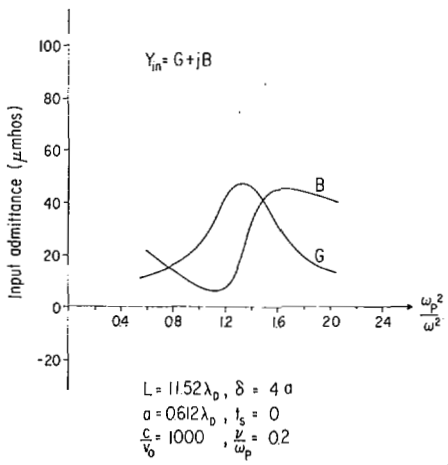

Fig. 12. Input admittance of dipole antenna in lossy warm plasma ($L = 11.52\lambda_D$, $\nu/\omega_p = 0.2$).

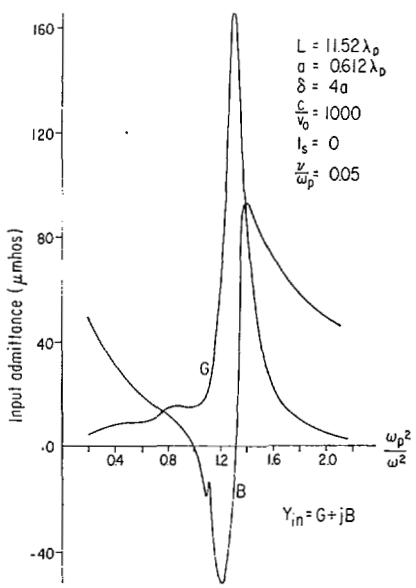

Fig. 13. Input admittance of dipole antenna in lossy warm plasma ($L = 11.52\lambda_D$, $\nu/\omega_p = 0.05$).

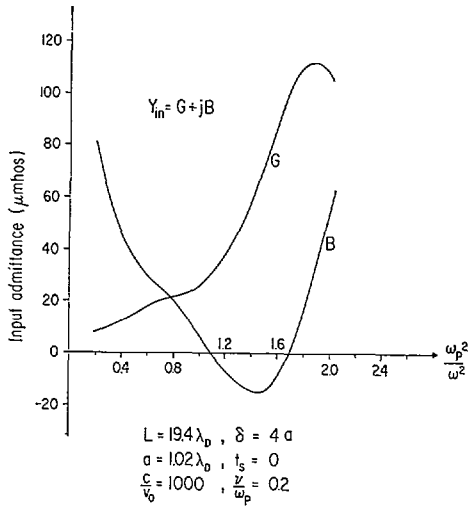

Fig. 14. Input admittance of dipole antenna in lossy warm plasma ($L = 19.40\lambda_D$, $\nu/\pi_p = 0.2$).

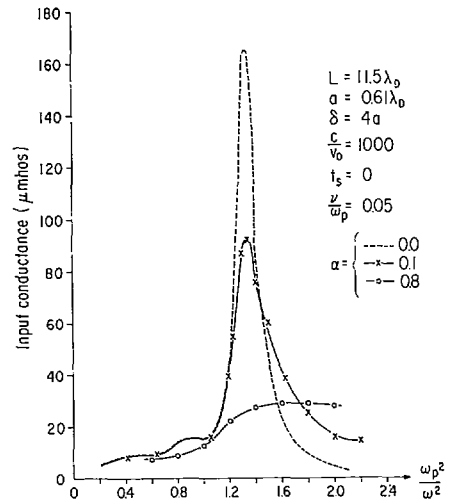

Fig. 15. Effect of absorptive surface on input conductance of dipole antenna in lossy warm plasma.

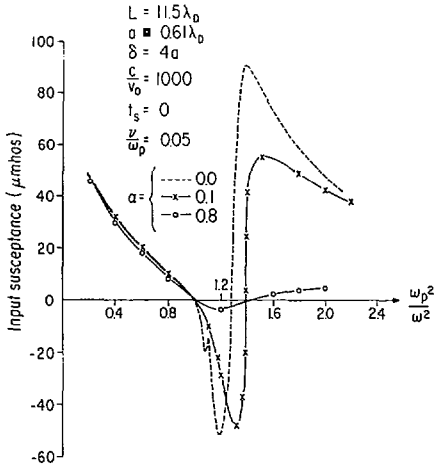

Fig. 16. Effect of absorptive surface on input susceptance of dipole antenna in lossy warm plasma.

by the work of Carlin and Mittra [15] who have shown that the total impedance Z_{in} contains a component Z_{JEM} due to the electromagnetic wave and a component Z_{JP} due to the electroacoustic wave. The reactive part of Z_{JEM} changes sign at $\omega_p^2/\omega^2 = 1$, but that of Z_{JP} does not. Since the electroacoustic wave is dominant when the antenna is short, the input reactance of a short antenna in compressible plasma may not change sign.

It is also important to note that the half-power width (in frequency band Δf) of these resonances is approximately equal to the collision frequency. From Fig. 14 we have $\Delta f/\omega_p = 0.22$, while $\nu/\omega_p = 0.2$, and from Fig. 13 we have $\Delta f/\omega_p = 0.062$, while $\nu/\omega_p = 0.05$. Experimental investigations of Waletzko and Bekefi [22], and Davies [23] have also indicated that $\Delta f \approx \nu$.

To recapitulate our findings we list the important features of a resonance probe as follows.

1) The resonance and antiresonance frequencies are below the plasma frequency.
2) The resonance and antiresonance frequencies are functions of antenna length.
3) The resonance may disappear if the antenna size is smaller than a few Debye length.
4) Resonance can occur with or without a sheath.
5) The collision effect may damp out the antiresonance at $\omega_p^2/\omega^2 = 1$ and the resonance below the plasma frequency.
6) The half-power width of the resonance is approximately equal to the collision frequency.

Effects of Absorptive Surface

The vacuum sheath around the antenna may collapse when the antenna is biased by a dc potential. This condition was studied by Wasserstrom, Su, and Probstein [24] who suggested that when the sheath is collapsed, the electron density is reasonably uniform right up to the surface, but there is a continuous flow of electrons to the surface. With that assumption Balmain [6], Wait [7] and Sancer [8] have used an absorptive boundary condition,

$$\hat{n} \cdot (\bar{v}/v_0) = \alpha(n_1/n_0)$$

for the plasma–metal interface. Figs. 15 and 16 show the effect of the absorption factor α on the input admittance of the antenna. It is evident that α has practically no effect on the input admittance at high frequency and very pronounced effect near resonance. Since the absorptive boundary condition is strictly hydrodynamic, it can have a significant influence on the input admittance of the antenna only when the plasma oscillation is dominated by the electroacoustic wave. The results of Figs. 15 and 16 are consistent with our previous conclusion that electroacoustic wave dominates when the antenna is short.

Conclusion

In this paper the boundary value problem posed by a sheathed finite antenna in an isotropic compressible and lossy plasma is solved. The results of this study have con-

firmed many findings of previous investigators and offer new information regarding the effects of sheath, loss, and absorptive surface on the radiation characteristic of the antenna. The analysis used in this paper is most useful for antennas which are electrically short but several plasma wavelengths in length. Because when the antennas are electrically short, the effects of the plasma compressibility and the absorptive surface are strong, the cold lossless sheathless plasma theory becomes unsatisfactory in predicting the antenna performance. We find such cases in the tenuous plasmas such as in the upper ionosphere, the solar wind, the interplanetary media, and in some laboratory experiments of tenuous plasmas where the probe may be of the size of several Debye lengths.

References

[1] S. H. Lin and K. K. Mei, "Numerical solution of dipole radiation in a compressible plasma," *IEEE Trans. Antennas Propagat.*, vol. AP-16, pp. 235–241, March 1968.

[2] J. Carlin and R. Mittra, "Acoustic waves and their effects on antenna impedance," *Can. J. Phys.*, vol. 45, pp. 1251–1269, March 1967.

[3] R. J. Lytle and F. V. Schultz, "Prolate spheroidal antennas in isotropic plasma media," *IEEE Trans. Antennas Propagat.*, vol. AP-17, pp. 496–506, July 1969.

[4] J. Wait and K. P. Spies, "Theory of a slotted-sphere antenna immersed in a compressible plasma, pt. III," *Radio Sci.*, vol. 1, p. 21, 1966.

[5] J. Galejs, "Insulated cylindrical antenna immersed in a compressible plasma," *Radio Sci.*, vol. 4, pp. 269–278, 1969.

[6] K. G. Balmain, "Impedance of a radio-frequency plasma probe with an absorptive surface," *Radio Sci.*, vol. 1, no. 1, pp. 1–12, 1966.

[7] J. R. Wait, *Electromagnetics and Plasmas*. New York: Holt, Rinehart and Winston, Inc., 1968.

[8] M. I. Sancer, "Boundary conditions for a unique solution to the linearized warm-plasma equations," *Radio Sci.*, vol. 1, no. 9, pp. 1067–1071, 1966.

[9] K. K. Mei, "Numerical methods in electromagnetic wave problems," class notes for presentation at Harry Diamond Lab., Washington, D. C., May 1968.

[10] S. H. Lin, "Dipole radiation in compressible plasma," Ph.D. dissertation, Dept. of Elec. Eng. and Computer Sciences, University of California, Berkeley, 1969.

[11] R. F. Harrington, *Field Computation by Moment Methods*. New York: Macmillan, 1968.

[12] F. B. Hildebrand, *Method of Applied Mathematics*, 2nd ed. Englewood Cliffs, N. J.: Prentice-Hall, 1965.

[13] R. W. P. King, *Theory of Linear Antennas*. Cambridge, Mass.: Harvard University Press, 1956.

[14] R. J. Lytle, "Linear antennas in plasma media," Ph.D. dissertation, Dept. of Elec. Eng., Purdue University, Lafayette, Ind., 1968.

[15] J. Carlin and R. Mittra, "Effects of induced acoustic sources on the impedance of a cylindrical dipole in a worm plasma," *Radio Sci.*, vol. 2, no. 11, pp. 1327–1338, 1967.

[16] J. E. Jackson and J. A. Kane, "Measurement of ionospheric electron densities using an RF probe technique," *J. Geophys. Res.*, vol. 64, pp. 1074–1075, August 1959.

[17] K. D. Baker and A. M. Despain, "Simultaneous comparison of RF probe techniques for determination of ionospheric electron density," *J. Geophys. Res.*, vol. 71, no. 3, pp. 935–944, 1966.

[18] R. S. Harp and F. W. Crawford, "Characteristics of the plasma resonance probe," *J. Appl. Phys.*, vol. 35, no. 12, pp. 3436–3446, 1964.

[19] J. A. Fejer, "Interaction of an antenna with a hot plasma and the theory of resonance probes," *Radio Sci.*, vol. 68D, no. 11, pp. 1171–1176, 1964.

[20] E. K. Miller, "The admittance of the infinite cylindrical antenna immersed in a lossy, compressible plasma," *IEEE Trans. Antennas Propagat.*, vol. AP-16, pp. 111–117, January 1968.

[21] E. K. Miller, "Admittance of an inhomogeneously sheathed infinite cylindrical antenna immersed in an isotropic, compressible plasma," *IEEE Trans. Antennas Propagat.* (Communications), vol. AP-16, pp. 501–502, July 1968.

[22] J. A. Waletzko and G. Bekefi, "RF admittance measurements of a slotted-sphere antenna immersed in a plasma," *Radio Sci.*, vol. 2, no. 5, pp. 489–493, 1967.

[23] P. G. Davies, "Laboratory studies of resonance retification," Science Research Council, Radio and Space Research Station, Slough, England, Rept. I.M. 242.

[24] E. C. Wassertrom, C. H. Su, and R. F. Probstein, "Kinetic theory approach to electrostatic probes," *Phys. Fluids*, vol. 8, no. 1, pp. 56–72, 1965.